Mainz Microtron MAMI

Collaboration A2: "Tagged Photons"
Spokesperson: A. Thomas

Proposal for an Experiment

"Polarisation observables using the Nucleon polarimeter with the Crystal Ball at MAMI"'

Collaborators:

> CrystalBall@MAMI collaboration

Spokespersons for the Experiment:
Dan Watts, Derek Glazier (University of Edinburgh), John Annand (University of Glasgow)

Abstract of Physics:
> The proton polarimeter used with the Crystal Ball at MAMI will be upgraded to make possible measurements of single and double polarisation observables with recoil neutrons and reactions with deuterium targets. The upgraded polarimeter design will exploit the planned multi wire proportional chamber tracker, the particle identification detector and the Crystal Ball, while at forward angles a new device comprising a segmented scintillator scatterer and the TAPS/TOF arrays will provide polarimetry information. The main goal of the experiment will be to obtain beam-recoil double polarisation observables for the π and η meson photoproduction channels up to $E_\gamma \sim 1.5$ GeV. The polarimeter will also allow first measurements of beam-recoil observables in multiple meson photoproduction. The transfer of polarisation to both the recoiling proton and neutron in Deuterium photodisintegration will be measured simultaneously.

Abstract of Equipment:
> The Glasgow-Mainz tagged photon spectrometer will be used with MAMI beam at the full MAMI-C energy. The Crystal Ball detector with TAPS as forward wall detector will be used to detect the photons from π^0 and η decays. The multi wire proportional chamber will be used in conjunction with the particle identification detector and graphite cylinder to construct the nucleon polarimeter. Forward angle polarimetry will be provided by a segmented scintillator scatterer with the TAPS / TOF arrays to detect the scattered nucleons

MAMI-Specifications:

beam energy	1557 MeV
beam current	< 100 nA
beam polarisation	polarized

Experiment–Specifications:

experimental hall/beam	A2
photon beam polarisation	linearly, circularly, unpolarized
detector	Crystal Ball, TAPS, MWPC, PID, TOF
target	5 cm liquid deuterium/hydrogen

Beam Time Request:

set–up/tests with beam	100 hours
data taking	960 hours

List of participating authors:

- **Institut für Physik, University of Basel, Switzerland**
  I. Jaegle, I. Keshelashvili, B. Krusche, Y. Maghrbi, F. Pheron, T. Rostomyan, D. Werthmüller

- **Institut für Experimentalphysik, University of Bochum, Germany**
  W. Meyer, G. Reicherz

- **Helmholtz–Institut für Strahlen- und Kernphysik, University of Bonn, Germany**
  R. Beck, A. Nikolaev

- **Massachusetts Institute of Technology , Cambridge, USA**
  A. Bernstein, W. Deconinck

- **JINR, Dubna, Russia**
  N. Borisov, A. Lazarev, A. Neganov, Yu.A. Usov

- **School of Physics, University of Edinburgh, UK**
  D. Branford, D.I. Glazier, T. Jude, M. Sikora, D.P. Watts

- **Petersburg Nuclear Physics Institute, Gatchina, Russia**
  V. Bekrenev, S. Kruglov, A. Koulbardis

- **Department of Physics and Astronomy, University of Glasgow, UK**
  J.R.M. Annand, D. Hamilton, D. Howdle, K. Livingston, J. Mancell, J.C. McGeorge, I.J.D. MacGregor, E.F. McNicoll, R.O. Owens, J. Robinson, G. Rosner

- **Department of Astronomy and Physics, Saint Mary's University Halifax, Canada**
  A.J. Sarty

- **Kent State University, Kent, USA**
  D.M. Manley

- **University of California, Los Angeles, USA**
  B.M.K. Nefkens, S. Prakhov, A. Starostin, I.M. Suarez

- **MAX-lab, University of Lund, Sweden**
  L. Isaksson

- **Institut für Kernphysik, University of Mainz, Germany**
  P. Aguar-Bartolome, H.J. Arends, S. Bender, A. Denig, E.J. Downie, N. Frömmgen, E. Heid, O. Jahn, H. Ortega, M. Ostrick, B.Oussena, P.B. Otte, S. Schumann, A. Thomas, M. Unverzagt

- **Institut für Physik, University of Mainz, D**
  J.Krimmer, W.Heil

- **University of Massachusetts, Amherst, USA**
  P.Martel, R.Miskimen

- **Institute for Nuclear Research, Moscow, Russia**
  G. Gurevic, R. Kondratiev, V. Lisin, A. Polonski

- **Lebedev Physical Institute, Moscow, Russia**
  S.N. Cherepnya, L.V. Fil kov, V.L. Kashevarov

- **INFN Sezione di Pavia, Pavia, Italy**
  A. Braghieri, A. Mushkarenkov, P. Pedroni

- **Department of Physics, University of Regina, Canada**
  G.M. Huber

- **Mount Allison University, Sackville, Canada**
  D. Hornidge

- **Tomsk Polytechnic University, Tomsk, Russia**
  A. Fix

- **Physikalisches Institut, University of Tübingen, Germany**
  P. Grabmayr, T. Hehl, D.G. Middleton
- **George Washington University, Washington, USA**
  W. Briscoe, T. Morrison, B.Oussena, B. Taddesse, M. Taragin
- **Catholic University, Washington, USA**
  D. Sober
- **Rudjer Boskovic Institute, Zagreb, Croatia**
  M. Korolija, D. Mekterovic, S. Micanovic, I. Supek

1   Introduction

The measurement of polarisation observables is a sensitive test for our understanding of reaction processes. In recent years the development of high intensity polarised photon beams and polarised nucleon targets has enabled a dramatic increase in the quality of experimental information available, which has been exploited for a host of physics goals to aid our understanding of non-perturbative QCD.

Here we propose measurements of the polarisation of recoil nucleons produced after photoreactions on the proton and deuterium targets. The successful development of the Phase-I proton polarimeter with the CB at MAMI is described and extensions to additionally enable neutron polarimetry with a Phase-II polarimeter is proposed.

The exploitation of the polarimeter in two main physics areas will be described. These are (i) pseudo-scalar meson photoproduction from the nucleon and (ii) deuterium photodisintegration. Both will be obtained with polarised photon beams. The central aim of the meson photoproduction experiments is to prove crucial new double-polarisation data from both the proton and neutron to obtain a full constraint of the complex helicity amplitudes. Better constraint on these amplitudes will lead to a better knowlege of the properties and existence of nucleon resonances via partial wave analyses. Additional information from beam-recoil observables in multiple meson production will be measured simultaneously.

In parallel with the meson production measurements on the neutron, double-polarisation beam recoil observables for deuterium photodisintegration will be obtained. These measurements will give new information to challenge recent state of the art theoretical descriptions of the deuteron and its disintegration to assess the accuracy of the nucleon meson description and give measurements sensitive to the onset of quark degrees of freedom in the reaction process.

1.1   Nucleon resonance spectrum

Detailed knowledge of the spectrum of nucleon resonances and the determination of their their mass, lifetime, quantum numbers and electromagnetic couplings give essential constraints on models of nucleon structure. However, accurate knowledge of this spectrum has remained elusive despite decades of study. The failure to fully establish this fundamental quantity is is a serious impediment in attempts to learn about how quarks interact to form nucleons. The resonance spectrum offers a fundamental test of theoretical models of the nucleon and its determination is central to establishing the appropriate dynamics and degrees of freedom in the nucleon. Description of the excitation spectrum is fundamental to undereatanding the structure of any composite system.

The current status of our knowledge the various nucleon resonances is outlined in Table 1, taken from the recent Baryon spectroscopy review by Klempt [1]. The resonances are classified according to a star rating which reflects the consistency with which signals for the resonance are observed in the various partial wave analyses. It is clear that there are many resonances within reach of MAMI-C which are poorly established because of inconsistent sightings, even though the different PWA analyses use largely the same experimental data. The main reason for this is the lack of a "complete" (see section 2.1) measurement of experimental observables in many channels. MAMI-C can reach centre of mass energies up to ∼1950 MeV which covers the masses of 6 uncertain (less than 4* rating) N*s and 3 uncertain Δ's. Additionally the broad widths of states with masses above the MAMI-C limit mean that data will have some sensitivity to their contribution. For example N* resonances with masses up to $\sim$2250 MeV/c^2 have full widths

typically of ∼350 MeV. The new data will also give new information the electromagnetic properties and isospin structure of resonances, which are not well constrained even for the better established states.

A variety of QCD inspired models have been formulated to attempt to describe the resonance spectrum of the nucleon. Constituent quark models predict a large number of resonances that have not yet been observed experimentally and it is not established if these states do not exist, or simply have not given sufficiently strong signals in the presently available experimental data. In the next decade significant progress is expected in less phenomenological theoretical descriptions of the nucleon resonance spectrum. In particular Lattice QCD calculations of the nucleon excitation spectrum are approaching the point where the light quark sector can be modelled realistically. calculations directly from QCD using Lattice techniques are starting to give predictions for the low-lying nucleon resonances using light quark masses which start to approach realistic values [2]. Also, there is the possibility of chiral symmetry restoration exhibited by the high lying and poorly established states[3]. Recently predictions of the nucleon excitation spectrum have been developed which are based on a holographic dual of QCD defined on an anti-de Sitter space, and which give a good description of the currently established spectrum [4]. In light of the theoretical advances already made, their expected development in future years and the current availability of high intensity photon beam facilities of appropriate energies it is very timely to improve our knowledge of this fundamental spectrum through a more complete measurement of observables in meson photoproduction.

1.2 Meson photoproduction from the nucleon

The photoproduction of pseudo-scalar mesons from the nucleon is described theoretically by 4 helicity amplitudes, which lead to 16 real experimental observables. The observables and their relation to the basic amplitudes are shown in Fig. 2.

Each observable has a different sensitivity to the underlying reaction amplitudes. To fully constrain these amplitudes without ambiguities requires the measurement of at least 8 observables which must be drawn from a combination of cross sections, single polarisation and a variety of double-polarisation observables. There has been significant experimental effort to determine these polarisation observables in recent years. Major programmes to measure beam-target double polarisation observables are in place at MAMI, JLAB, ELSA and GRAAL where measurements of E and G have taken data or are planned and measurements of F anf H are expected with the availability of transversely polarised targets. Very importantly however, a full constraint of the amplitudes also requires measurement of double polarisation observables involving recoil polarisation and the proposed programme here will therefore play a crucial role in this world programme. The MAMI facility has the highest tagged-photon beam intensity of any current facility and is ideally suited to produce a sufficently large event sample to enable recoil polarimetry determination, for which detection efficiency is necessarily low.

Each measurement of a double-polarisation observable gives information on a different bi-linear combination of the helicity amplitudes and has the potential to significantly affect the PWA solution (see Fig. 2). A recent prediction of the effectiveness of double-polarisation observables with recoil polarisation is seen in Ref.[6] where double-polarisation measurements with circular polarised beam and recoil nucleon polarisation are predicted to be particularly effective in revealing some of the poorly established resonances. Beam-target polarised data obtained recently have already shown their worth. For example recent measurements of the E observable with circularly polarised beam and polarised target indicate the need for revised photocouplings for

TABLE XIII Breit-Wigner masses W_R and widths Γ (in MeV) of N and Δ resonances.

Resonance	Our estimate	Our rating	KH	CM	Kent	GWU	BnGa
$N_{1/2^+}(1440)$	1440±30; 300±100	****	1410±12; 135±10	1440±30; 340±70	1462±10; 391±34	1485± 1; 284±18	1436±15; 335±40
$N_{3/2^-}(1520)$	1520± 5; 115±10	****	1519± 4; 114± 7	1525±10; 120±15	1524± 4; 124± 8	1516± 1; 99± 3	1524± 5; 112±10
$N_{1/2^-}(1535)$	1535±10; 150±25	****	1526± 7; 120±20	1550±40; 240±80	1534± 7; 151±27	1547± 1; 188± 4	1530±30; 210±30
$N_{1/2^-}(1650)$	1655±15; 165±30	****	1670± 8; 180±20	1650±30; 150±40	1659± 9; 170±12	1635± 1; 115± 3	1705±30; 220±30
$N_{5/2^-}(1675)$	1675± 5; 150±20	****	1679± 8; 120±15	1675±10; 160±20	1676± 2; 159± 7	1674± 1; 147± 1	1670±20; 140±40
$N_{5/2^+}(1680)$	1685± 5; 130±10	****	1684± 3; 128± 8	1680±10; 120±10	1684± 4; 139± 8	1680± 1; 128± 1	1667± 6; 102±15
$N_{3/2^-}(1700)$	1700±50; 100±50	***	1731±15; 110±30	1675±25; 90±40	1737±44; 250±230	-	1740±20; 180±30
$N_{1/2^+}(1710)$	1710±30; 150±60	**	1723± 9; 120±15	1700±50; 90±30	1717±28; 480±330	-	-
$N_{3/2^+}(1720)$	1720±30; 200±80	****	1710±20; 190±30	1700±50; 125±70	1717±31; 380±180	1750± 5; 256±22	1720±30; 330±60
$N_{3/2^-}(1860)$	1860±40; 200±100	**	-	1880±100; 180±60	1804±55; 450±185	-	1875±25;105±25
$N_{1/2^+}(1880)$	1880±40; 200±100	*	-	-	1885±30; 113±44	-	1880±40; 220±60
$N_{5/2^+}(1890)$	1890±50; 300±150	**	1882±10; 95±20	-	1903±87; 490±310	-	1880±30; 250±50
$N_{3/2^+}(1900)$	1900±70; 350±150	*	-	-	1879±17; 498±78	-	1915±50; 220±65
$N_{1/2^-}(1905)$	1905±60; 250±150	*	1880±20; 95±30	-	1928±59; 414±157	-	-
$N_{7/2^+}(1990)$	1990±80; 380±160	**	2005±150; 350±100	1970±50; 350±120	2086±28; 535±120	-	-
$N_{3/2^-}(2080)$	2090±50; 300±100	$\overline{**}$	2080±20; 265±40	2060±80; 300±100	-	-	2160±40; 340±65
$N_{1/2^-}(2090)$	2180±80; 350±100		-	2180±80; 350±100	-	-	-
$N_{1/2^+}(2100)$	2100±100; 300±200	*	2050±20; 200±30	2125±75; 260±100	-	-	-
$N_{5/2^-}(2200)$	2150±80; 340±160	*	2228±30; 310±50	2180±80; 400±100	-	-	2060±30; 340±50

			KH	CM	Kent	GWU	Hendry
$N_{7/2^-}(2190)$	2170±50; 390±120	****	2140±12; 390±30	2200±70; 500±150	2127± 9; 550±50	2152±2; 484±13	2140±40; 270±50
$N_{9/2^+}(2220)$	2260±60; 500±150	****	2205±10; 365±30	2230±80; 500±150	-	2316±3; 633±17	2300±100; 450±150
$N_{9/2^-}(2250)$	2250±50; 400±120	****	2268±15; 300±40	2250±80; 400±120	-	2302±6; 628±28	2200±100; 350±100
$N_{11/2^-}(2600)$	2630±150; 650±300	***	2577±50; 400±100	-	-	-	2700±100; 900±100
$N_{13/2^+}(2700)$	2800±160; 600±300	**	2612±45; 350±50	-	-	-	3000±100; 900±150

			KH	CM	Kent	GWU	BnGa
$\Delta_{3/2^+}(1232)$	1232± 1; 118± 2	****	1232± 3; 116± 5	1232± 2; 120± 5	1231± 1; 118± 4	1233± 1; 119± 1	1231± 4; 114± 5
$\Delta_{3/2^+}(1600)$	1625±75; 350±100	****	1522±15; 220±40	1600±50; 300±100	1706±10; 430±73	-	1620±80; 350±100
$\Delta_{1/2^-}(1620)$	1630±30; 140±10	****	1610± 7; 139±18	1620±20; 140±20	1672± 7; 154±37	1614±1; 71±3	1650±25; 250±60
$\Delta_{3/2^-}(1700)$	1710±40; 300±100	****	1680±70; 230±80	1710±30; 280±80	1762±44; 600±250	1688±3; 182±8	1640±40; 270±60
$\Delta_{1/2^+}(1750)$			-	-	1744±36; 300±120	-	-
$\Delta_{1/2^-}(1900)$	1900±50; 190±50	**	1908±30; 140±40	1890±50; 170±50	1920±24; 263±39	-	-
$\Delta_{5/2^+}(1905)$	1890±25; 330±70	****	1905±20; 260±20	1910±30; 400±100	1881±18; 327±51	1856± 2; 321± 9	1800±50; 370±110
$\Delta_{1/2^+}(1910)$	1895±25; 280±50	****	1888±20; 280±50	1910±40; 225±50	1882±10; 229±25	2068±2; 543±10	-
$\Delta_{3/2^+}(1920)$	1940±60; 240±80	***	1868±10; 220±80	1920±80; 300±100	2014±16; 152±55	-	1990±35; 330±60
$\Delta_{5/2^-}(1930)$	1960±60; 360±140	**	1901±15; 195±60	1940±30; 320±60	1956±22; 530±140	-	-
$\Delta_{3/2^-}(1940)$	1990±60; 300±100	$\overline{**}$	-	1940±100; 200±100	2057±110; 460±320	-	1990±40; 410±70
$\Delta_{7/2^+}(1950)$	1920±25; 285±50	****	1913± 8;224±10	1950±15; 340±50	1945± 2; 300± 7	1921± 1; 271± 1	1895±20; 260±40
$\Delta_{5/2^+}(2000)$			2200±125; 400±125	-	1752±32; 251±93	-	-
$\Delta_{1/2^-}(2150)$			-	2200±100; 200±100	-	-	-

			KH	CM	Kent	GWU	Hendry
$\Delta_{7/2^-}(2200)$	2240±60; 400±100	**	2215±10; 400±100	2200±80; 450±100	-	-	2280±80; 400±150
$\Delta_{9/2^+}(2300)$	2350±80; 400±100	**	2217±80; 300±100	2400±125; 425±150	-	-	2450±100; 500±200
$\Delta_{3/2^-}(2350)$	2350±50; 300±70	***	2305±26; 300±70	2400±125; 400±150	-	2233±53; 773±187	-
$\Delta_{7/2^+}(2390)$	2390±100; 300±100	*	2425±60; 300±80	2350±100; 300±100	-	-	-
$\Delta_{9/2^-}(2400)$	2400±100; 400±200	**	2468±50;480±100	2300±100; 330±100	-	2643±141; 895±432	2200±100; 450±200
$\Delta_{11/2^+}(2420)$	2400±50; 400±100	***	2416±17; 340±28	2400±125; 450±150	-	2633±29; 692±47	2400±60; 460±100
$\Delta_{13/2^-}(2750)$	2750±100; 420±200	**	2794±80; 350±100	-	-	-	2650±100; 500±100
$\Delta_{15/2^+}(2950)$	2920±100; 500±200	**	2990±100; 330±100	-	-	-	2850±100; 700±200

Figure 1: Breit Wigner masses and widths in MeV of N and Δ resonaonces

Observable	Polarisation of γ	target	recoil	
1. $\{d\sigma/d\Omega\}/\mathcal{N}$				$=|b_1|^2+|b_2|^2+|b_3|^2+|b_4|^2$
Single polarization				
2. P			y'	$=|b_1|^2-|b_2|^2+|b_3|^2-|b_4|^2$
3. Σ	p			$=|b_1|^2+|b_2|^2-|b_3|^2-|b_4|^2$
4. T		y		$=|b_1|^2-|b_2|^2-|b_3|^2+|b_4|^2$
Double polarizaton				
Beam-target				
5. E	c	z		$=2\,\mathrm{Re}(b_1 b_3^* + b_2 b_4^*)$
6. F	c	x		$=2\,\mathrm{Im}(b_1 b_3^* - b_2 b_4^*)$
7. G	t	z		$=2\,\mathrm{Im}(b_1 b_3^* + b_2 b_4^*)$
8. H	t	x		$=-2\,\mathrm{Re}(b_1 b_3^* + b_2 b_4^*)$
Beam-recoil				
9. C_x	c		x'	$=-2\,\mathrm{Im}(b_1 b_4^* - b_2 b_3^*)$
10. C_y	c		z'	$=2\,\mathrm{Re}(b_1 b_4^* + b_2 b_3^*)$
11. O_x	t		x'	$=2\,\mathrm{Re}(b_1 b_4^* - b_2 b_3^*)$
12. O_z	t		z'	$=2\,\mathrm{Im}(b_1 b_4^* + b_2 b_3^*)$
Target-recoil				
13. T_x		x	x'	$=2\,\mathrm{Re}(b_1 b_2^* - b_3 b_4^*)$
14. T_z		x	z'	$=2\,\mathrm{Im}(b_1 b_2^* - b_3 b_4^*)$
15. L_x		z	x'	$=-2\,\mathrm{Im}(b_1 b_2^* + b_3 b_4^*)$
16. L_z		z	z'	$=2\,\mathrm{Re}(b_1 b_2^* + b_3 b_4^*)$

Figure 2: The 16 measurable quantities in pseudo-scalar meson photoproduction and their relation to the 4 basic reaction amplitudes b_1 to b_4

even 'well established resonances such as the $D_{13}(1520)$[5]. The E measurements gave some of the first constraints on the real part of the intereferences between the amplitudes. The double-polarisation measurements proposed here will give some of the first strong constraints on the imaginary parts of the interference terms between the amplitudes (e.g. C_x).

To disentangle the resonances and their electromagnetic properties it is vital to measure polarisation observables, both for different final states and for proton and neutron targets. This arises from the nature of the photproduction amplitude. Obviously, it is desirable to measure from proton and neutron targets as different resonances have different coupling to the proton or neutron. The photon field has isoscalar ($A^{(0)}$) and isovector ($A^{(1)}$) components which contribute to the photoproduction amplitude as follows:

$$A_{\gamma p \longrightarrow \pi^0 p} = -\left[\frac{1}{3}A_{\pi N}^{(0)} - \frac{1}{3}A_{\pi N}^{(1)}\right]^{I=\frac{1}{2}} + \frac{2}{3}A_{\pi N}^{I=\frac{3}{2}}$$

$$A_{\gamma p \longrightarrow \pi^+ n} = \frac{1}{\sqrt{2}}\left[\frac{1}{3}A_{\pi N}^{(0)} - \frac{2}{3}A_{\pi N}^{(1)}\right]^{I=\frac{1}{\sqrt{2}}} + \frac{2}{3}A_{\pi N}^{I=\frac{3}{2}}$$

$$A_{\gamma n \longrightarrow \pi^0 n} = \left[\frac{1}{3}A_{\pi N}^{(0)} + \frac{1}{3}A_{\pi N}^{(1)}\right]^{I=\frac{3}{2}} + \frac{2}{3}A_{\pi N}^{I=\frac{3}{2}}$$

$$A_{\gamma n \longrightarrow \pi^- p} = -\frac{1}{\sqrt{2}}\left[\frac{1}{3}A_{\pi N}^{(0)} + \frac{1}{3}A_{\pi N}^{(1)}\right]^{I=\frac{1}{2}} + \frac{\sqrt{2}}{3}A_{\pi N}^{I=\frac{3}{2}}$$

The components $A^{(0)}$ and $A^{(1)}$ result from coupling of the I$=\frac{1}{2}$ nucleon to the isoscalar and isovector component of the photon to yield a total isospin of $\frac{1}{2}$. Measurements of $\gamma p \rightarrow p\pi^0$

and $\gamma p \rightarrow n\pi^+$ are sufficient to extract the I=$\frac{3}{2}$ amplitudes. However A$^{(0)}$ and A$^{(1)}$ can only be disentangled with data on both proton and neutron targets.

With the recoil polarimeter we will access for pseudo-scalar meson photoproduction (π and η) the double polarisation observables C$_x$ (circularly polarised photon beam + recoil) and O$_x$ (Linearly polarised photon beam + recoil), the single polarisation observable P and the transverse target observable T (this is accessible from the y component of nucleon polarisation with a linearly polarised photon beam). The latter will give complimentary measurement to the cross check measurements made with a transversely polarised target.

The measurements will be achieved for both proton and neutron targets and with both protons and neutrons as the final state particles. These measurements will in several cases be the first measurement of a particular observable. Otherwise they will greatly extend the precision and kinematic range of existing measurements. The data will be a vital addition to the currently active world programme of beam-target double polarisation measurements at MAMI, JLAB and ELSA. Combining the beam-recoil and beam-target results will enable the first measurement of a complete set of observables, reaching the 8 observables necessary to strongly constrain PWA and improve our understanding of the nucleon resonances.

Simultaneously measurements of beam-recoil observables in 2-meson production (both $\pi\pi$ and $\eta\pi$) will be obtained. The framework for double pseudo-scalar meson production involves more amplitudes and there are correspondingly more observables. The formalism for these observables was recently described by Roberts et. al. [7]. As part of our proposed programme we will obtain the first measurement of beam-recoil observables in these reactions, which will be a valuable and unique addition to the data emerging from the programme of beam-recoil, single-spin and beam asymmetry measurements for double-meson photoproduction at MAMI, JLAB and ELSA.

1.3 Meson photoproduction - Previous experiments

1.3.1 Neutral pion photoproduction

There are currently no measurements of double polarisation observables or single polarisation observables P or T for neutral pion photoproduction from the neutron.

The world's $p(\gamma, p)\pi^0$ data for the observables accessible in the proposed experiment are shown in Fig. 3. The data taken at all production angles are included. It is clear that there is a reasonable number of measurements of the single polarisation observables P and T, mainly obtained in the 70's and 80's. These data will be a useful cross check of our experiment and we will add new high quality data to the data base.

The experimental situation is significantly worse for the double-polarisation data. There have been some pioneering measurements of O$_{x'}$ at Kharkov and Yerevan[11], but the statistical accuracy and kinematic coverage is rather poor. There is a recent measurement of C$_{x'}$ (circular polarised photon beam + recoil) by the Hall A collaboration at Jefferson Lab[8], with restricted angle and discrete E_γ in the range $0.8 - 4$ GeV. The $p(\gamma, p)\pi^0$ reaction was identified by determination of the proton energy and angle in a magnetic spectrometer. The observables C$_{x'}$, C$_{z'}$ and P were measured although the data were taken mainly at high photon energies to look for signals of the onset of perturbative QCD.
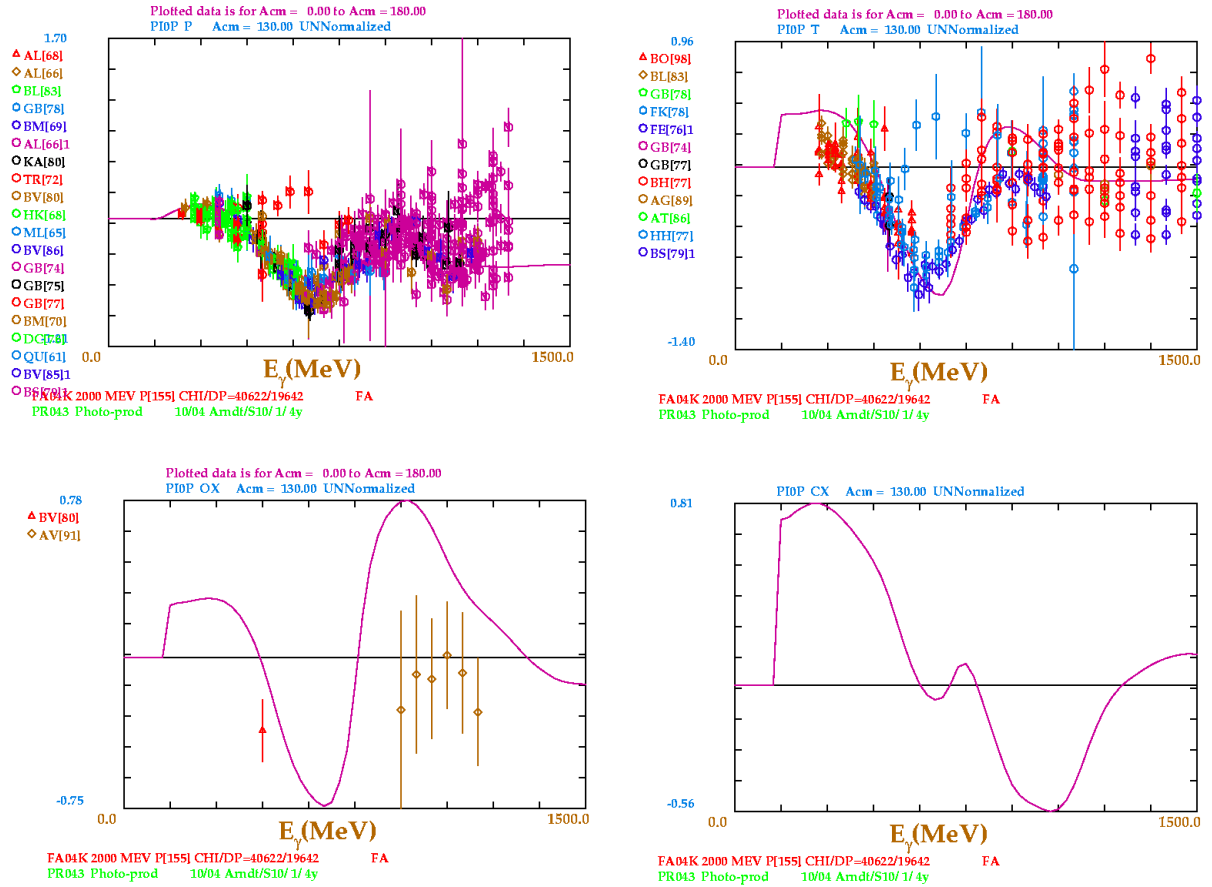
Figure 3: World's P,T O_x and C_x experimental data for $p(\gamma, p)\pi^0$ at all CM production angles. Clockwise from top left are shown P, T, $O_{x'}$ and C_x, as a function of E_γ from the SAID[12] database. The line shows the SAID predictions at a CM production angle of 135^0. (The recent $C_{x'}$ data[8] is not shown on the figure)
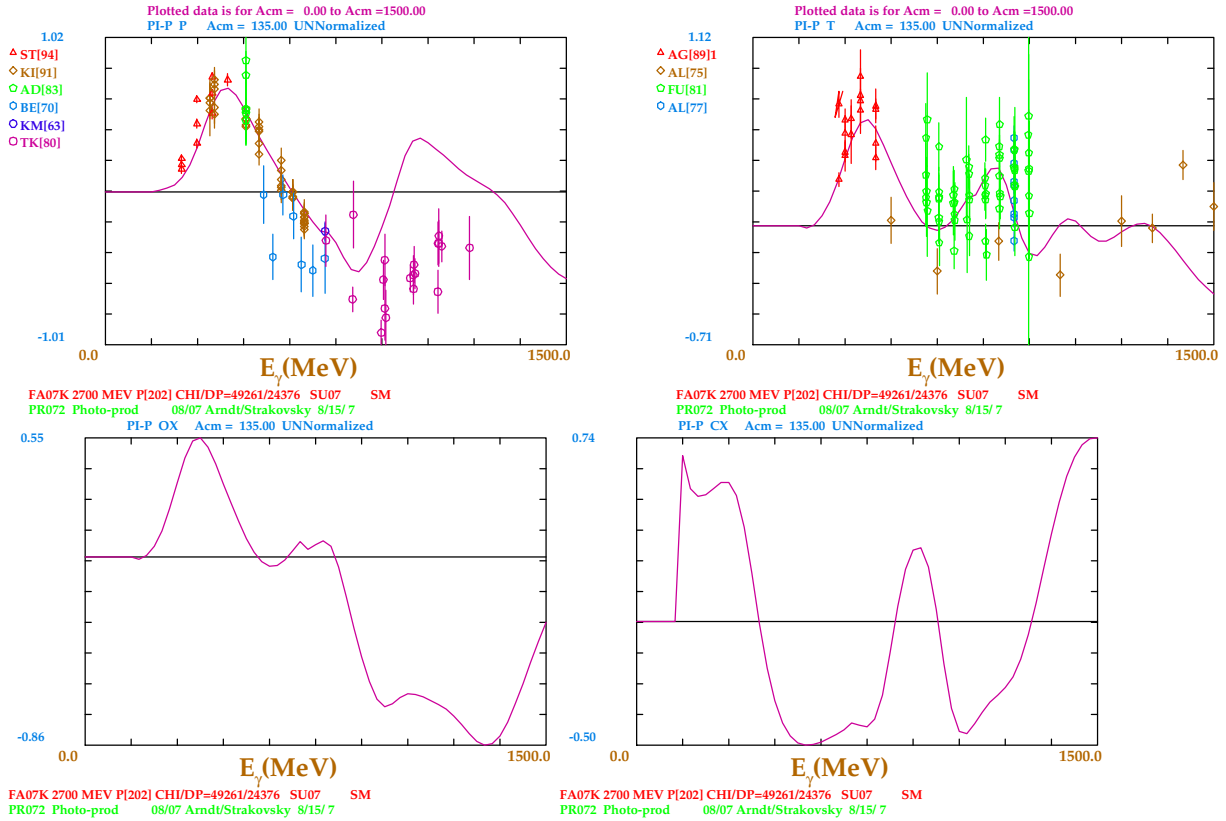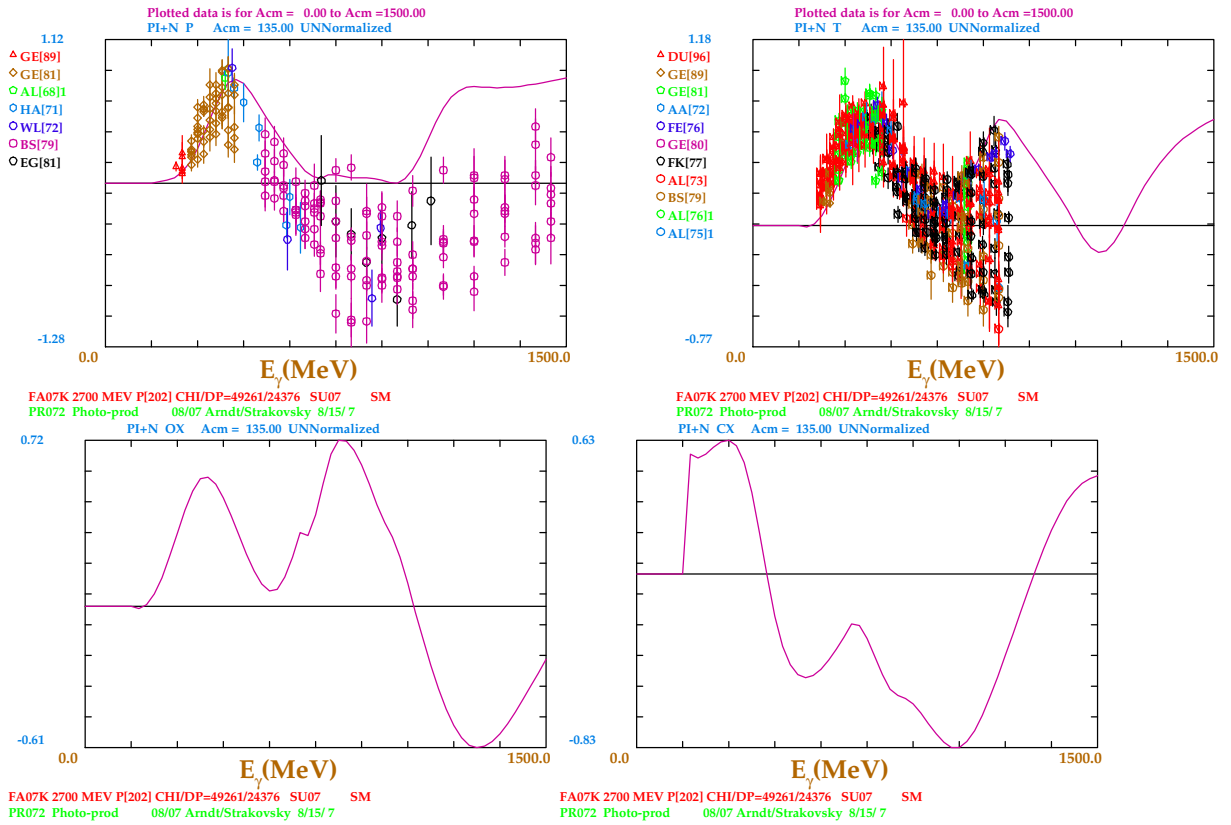
Figure 4: World's experimental data for $n(\gamma, p)\pi^-$ at all CM production angles. Clockwise from top left are shown P, T, $O_{x'}$ and C_x, as a function of E_γ from the SAID database. The line shows the SAID predictions at a CM production angle of 135^0

1.3.2 Charged pion photoproduction

There have been some measurements of the single polarisation observables P, T for both charged pion production channels. The world data are shown in figure 4 and 5. There has been no measurement of a beam-recoil double polarisation observable for these reactions and the measurements proposed here will be particularly valuable.

1.3.3 η photoproduction

There are no published measurements of any beam-recoil observable for η photoproduction. The target asymmetry (T) has been measured recently at ELSA[9] and the linear polarisation observable Σ has been obtained at ELSA and GRAAL[10]. Measurement of the beam-target observable G is planned or under analysis at JLAB, ELSA and MAMI.

There has been particular interest on the eta photoproduction from the neutron because of indications of narrow structure in the cross section. Interpretations of this structure in terms of a new narrow resonance ($P_{11}(1685)$) or as the interference of known resonances is currently under debate. Clearly more complete measurements of observables in this region will help to constrain the partial wave analysis in this region to better establish whether the interference interpretation is plausible. Particular sensitivity to the inclusion of the narrow resonance is predicted in P, T and O_x [15].

Figure 5: World's experimental data for $p(\gamma, n)\pi^+$ at all CM production angles. Clockwise from top left are shown P, T, $O_{x'}$ and C_x, as a function of E_γ from the SAID database. The line shows the SAID predictions at a CM production angle of 135^0

1.4 Deuterium photodisintegration

There are also possibilities to exploit the nucleon polarimeter to obtain beam-recoil polarisation measurements in deuterium photodisintegration. There are some data on C_x for the final state proton for $\theta_{cm} = 90°$ using the magnetic spectrometer of hall-A [20]. The spectrometer technique cannot measure the polarisation transfer to recoil neutron and is difficult to achieve large angular and energy coverage as each data point requires a separate run with different spectrometer settings and beam energy.

There have been some pioneering measurements of the transfer of polarisation fom a linearly polarised beam by the Kharkov group in the 80's[23]. However the results had rather poor statistical accuracy and are limited in both photon energy and angular coverage.

We will carry out a measurement of polarisation transfer to both proton and neutron in the final state, with a large angular coverage and for both linear and circularly polarised photons. The data will challenge the state-of-the-art nucleonic descriptions of Deuteron photodisintegration [18] which use latest NN potentials and include relativistic effects. This model has been very succesful in accuractely describing many observables in the disintegration process, however the recoil polarisation P is still not described.

At higher photon energies new data to challenge the proposed low energy transition from nucleon to quark degrees of freedom at $E_\gamma \sim 1$ GeV will be obtained. This transition has been suggested by recent JLAB measurements of the proton polarisation in photodisintegration from circularly polarised photons [20].

2 The proposed experiment

2.1 Extraction of polarisation observables from the data

The differential cross section including recoil polarisation for pseudoscalar photoproduction, with a polarised photon beam, can be expressed as:

$$
\begin{aligned}
\rho_f \frac{d\sigma}{d\Omega} &= \frac{d\sigma}{d\Omega_0} \left[\, 1 - P_\gamma^{lin}\Sigma\cos 2\phi_m + \sigma_{x'}\left(P_\gamma^{circ}C_{x'} + P_\gamma^{lin}O_{x'}\sin 2\phi_m\right) \right. \\
&\quad \left. + \sigma_{y'}\left(P - P_\gamma^{lin}T\cos 2\phi_m\right) + \sigma_{z'}\left(P_\gamma^{circ}C_{z'} + P_\gamma^{lin}O_{z'}\sin 2\phi_m\right)\,\right]
\end{aligned}
\tag{1}
$$

where, P_γ^{lin} and P_γ^{circ} are the linear and circular polarisation of the beam; ϕ_m is the azimuthal angle of the meson in the lab. frame; and the matrices, $\sigma_{x',y',z'}$ refer to the nucleon quantisation axes defined by:

$$
\widehat{z'} = \widehat{p}_p \quad \widehat{y'} = \frac{p_\gamma \times p_m}{|p_\gamma \times p_m|} \quad \widehat{x'} = \widehat{y'} \times \widehat{z'}
$$

where p_γ, p_p and p_m are the momentum of the beam, recoil nucleon and meson respectively. The Σ, P, T, O_x and C_x observables will be simultaneously extracted from the experimental data.

The beam asymmetry Σ is measured with a linearly polarised beam having a known degree of polarisation (P_γ^{lin}) . The resulting asymmetry in the meson azimuthal distribution, $N(\phi_m)$, can be fitted with a $\cos(2\phi_m)$ function, the amplitude of which is equal to the product $P_\gamma^{lin}\Sigma$. The P, T, O_x and C_x require information from the nucleon polarimeter. Summing the different photon beam polarisations to give an effective unpolarised beam will allow us to access the single

polarisation observable P. Denoting the scattered proton azimuthal angle as ϕ'_p, the product of the polarimeter analysing power and induced nucleon polarisation, AP, can be extracted from the amplitude of a $\cos\phi'_p$ fit to the azimuthal angular distribution corrected for detector acceptance.(the x-component of nucleon polarisation will be zero as shown in equation 1).

Further polarisation observables are accessed utilising the citcularly polarised photon beam capabilities at MAMI in conjunction with our nucleon polarimeter. Forming asymmetries from the different beam helicity states will cancel the acceptances of the nucleon polarimeter. The circular polarised beam-recoil observable C_x can be measured from the azimuthal asymmetry:

$$\frac{N^+\left(\phi'_p\right) - N^-\left(\phi'_p\right)}{N^+\left(\phi'_p\right) + N^-\left(\phi'_p\right)} = \frac{C_{x'}P_\gamma^{circ}A\sin\phi'_p}{1 + AP cos(\phi'_p)} \tag{2}$$

where the $\pm$ refers to the helicity of the beam and A is the analysing power of the polarimeter. It can be seen from equation 1 that the y-component of nucleon polarisation is insensitive to the helicity of the photon beam.

O_x and T are measured simultaneously using a beam of linearly polarised photons. As seen in eqn. 1 this polarisation rotates with the meson azimuthal angle and in order to extract $O_{x'}$ and T we construct an asymmetry that is a function of both ϕ_m and ϕ'_p:

$$\frac{N^\perp\left(\phi_m, \phi'_p\right) - N^\|\left(\phi_m, \phi'_p\right)}{N^\perp\left(\phi_m, \phi'_p\right) + N^\|\left(\phi_m, \phi'_p\right)} = \frac{AP_\gamma^{lin}\left(O_{x'}\sin 2\phi_m \sin\phi'_p + T\cos 2\phi_m \cos\phi'_p\right) - P_\gamma \Sigma \cos 2\phi_m}{1 + AP\cos\phi_p}$$

$$\tag{3}$$

where the $\|$, $\perp$ refer to the direction of linear polarisation. The beam asymmetry, Σ, will be determined with ~50 times the statistics of O_x and so can be removed from equation 3 and has a negligible contribution to the uncertainty in O_x. The extraction of O_x proposed here has since been succesfully adopted in the analysis of strangeness photoproduction at JLAB [16] and GRAAL[24].

The techniques for extraction of beam-recoil observables in deuterium photodisintegation are similar to those highlighted for meson photoproduction, where the meson angle is replaced by the nucleon angle.

2.2 Analysing powers

2.2.1 The ^{12}C(p,p$^/$) reaction

The analyzing power is well established for this reaction as graphite is often used as the analysing material in polarimeters. Figure 6 shows a fit to the available ^{12}C(p,p$^/$) analyzing power experimental data, plotted as a function of proton scattering angle and the proton energy. This new parameterisation includes experimental data taken up to 2009 and was carried out by the proposers for use in the analysis of the phase-I polarimeter.

2.2.2 The ^{12}C(n,p) reaction

Previous measurements indicate that the analysing power for the ^{12}C(n,p) reaction follows closely that of the ^{1}H(n,p) reaction i.e. where the quasi-free process dominates so binding effects are
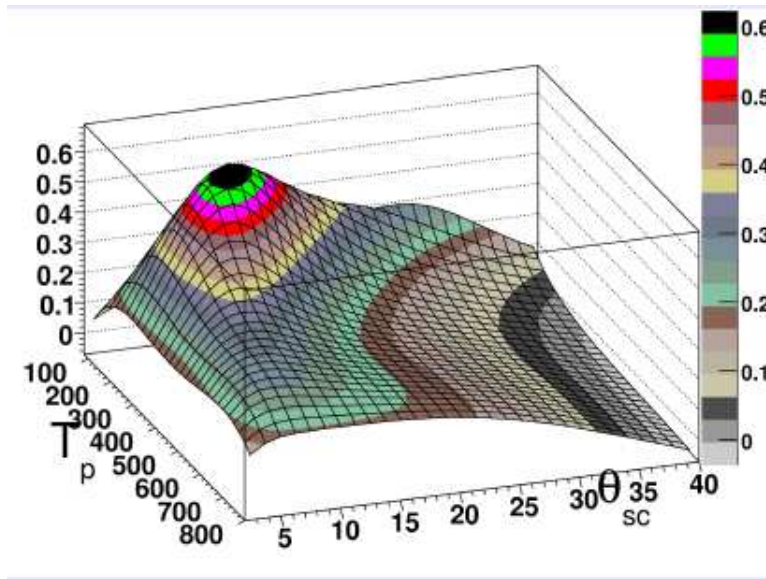
Figure 6: 2D surface showing the parameterisation of the analysing power for ^{12}C(p,p$^/$) reaction plotted as a function of proton scattering angle (degrees) and proton energy (MeV).
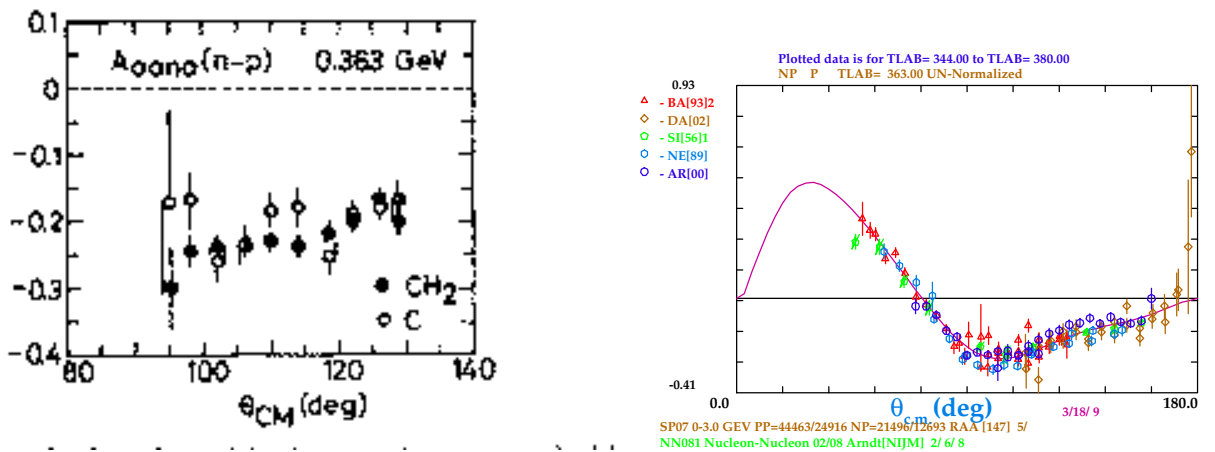

Figure 7: Left panel: Analysing power for ^{12}C(n,p) (open circles) and $CH_2(n,p)$ closed circles) for T_p=0.368 GeV[?]. Right panel: Analyzing power from SAID PWA [12] for reaction on free nucleon at the same energy

small. For example, a Saclay[17] measurement for nucleon energies close to the middle of our detected range for the polarimeter is shown in Fig. 7. Recent work for the NPOL3 spectrometer also confirms this observation [25]. For the analysis of the ^{12}C(n,p) scatters we will therefore adopt the analyzing powers extracted from the PWA solution of (n,p) scattering. Similar assumptions on the dominaince of the quasi-free analysing powers were made for the neutron polarimetry on ^{12}C carried out at Yerevan [11] analyzing ^{12}C(n,n).

2.3 Phase-I Nucleon polarimeter design

The proton polarimeter was commissioned in test beamtimes and production beamtimes on liquid hydrogen in 2007/2008. This Phase-I design is shown in Fig. 8 and utilises the Particle identification scintillator barrel (PID), inside a 2cm thick graphite cylinder. The phase-I device was designed to give polarisation information on protons.

The operation of the phase 1 polarimeter relies on kinematic reconstruction. Protons incident on the graphite which undergo nuclear interactions are isolated by reconstructing their scattering angle in the graphite. This is determined from the reconstructed incident proton 4-vector, the calculation of which uses the incoming tagged photon 4-vector and the measured meson 4-vector. The scattered nucleon angle is determined from the hit position of the scattered proton in the ball.

The measured scattering angle in the graphite from the experimental data is shown in Fig 9, compared to a GEANT4 (G4) simulation of the apparatus which includes the realistic energy and angle resolutions of the detector. Very good agreement is observed for the reconstructed scatter angles. The G4 prediction without the inclusion of nuclear scatter events in the event tracking is also shown in the figure and illustrates the rather good rejection of these background events with a simple cut on scatter angle larger than $\sim 12°$. These background events largely arise from multiple coulomb scattering of the protons, and the width of the peak is largely determined by the angular resolution in the reconstruction of the scatter angle. These uncertainties arise from the granularity of the nucleon detector, the thickness of the scattering material and the angular resolution for the reconstruction of the incident proton. The necessary minimum scatter angle cut of $\sim 12°$ is similar to the minimum angle achievable with polarimeters which including tracking devices (e.g. the focal plane polarimeter in A1[21], JLAB Hall A [22])

2.3.1 Phase-I polarimeter - preliminary results

The preliminary analysis of the beam-recoil observable C_x for the p(γ, π^0) reaction using data from the first stage of production running with the Phase-I polarimeter is shown in Figure 10. The analysis corresponds to $\sim$250 hours of beam on target. Good agreement with the sparse available JLAB data is observed. Even in the region of the low lying resonances the new data indicate the present solution of the SAID partial wave analysis from the GWU group does not predict the right sign or magnitude for the observable.

The preliminary analysis of C_x for the p($\gamma, p\eta$) reaction is shown in fig 11. Even in the region near threshold where this reaction is dominated by the $S_{11}(1535)$ the SAID and MAID partial wave analyses give very different predictions fo this observable highlighting the poor constraint of PWA for this reaction. The preliminary C_x data clearly favour the current solution of SAID, illustrating the sensitivity of the new data. With the remainder of the beam allocation for the phase-I polarimeter we hope to improve the statistical accuracy of the results for the η.
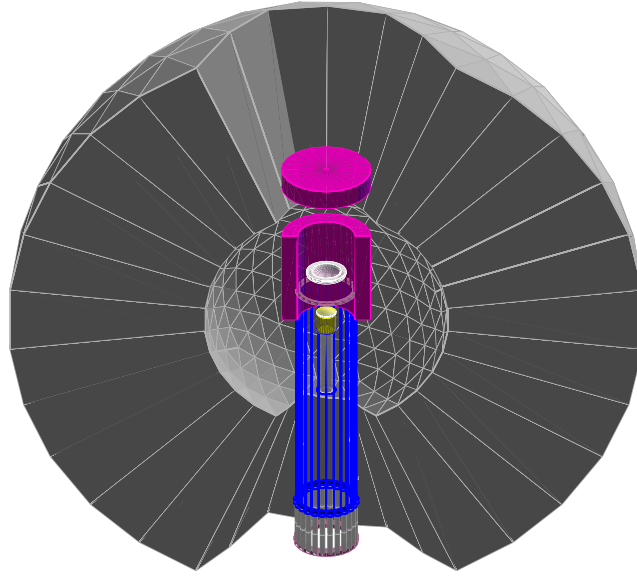
Figure 8: Schematic of the design of the phase-I polarimeter. The PID is shown in blue, the graphite in pink. Hydrogen target cell and feed pipes in yellow. The incident photon beam direction runs from bottom to top.
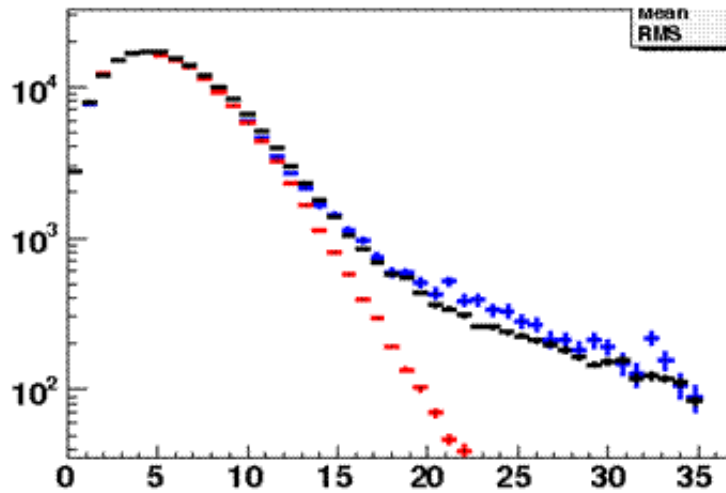

Figure 9: Measured distribution of the scatter angle in the analysing graphite (Black markers). The G4 simulation including nuclear interactions and excluding nuclear interactions are shown as the blue and red markers respectively. Results are for θ_{pi}=** and for E_γ=** to **
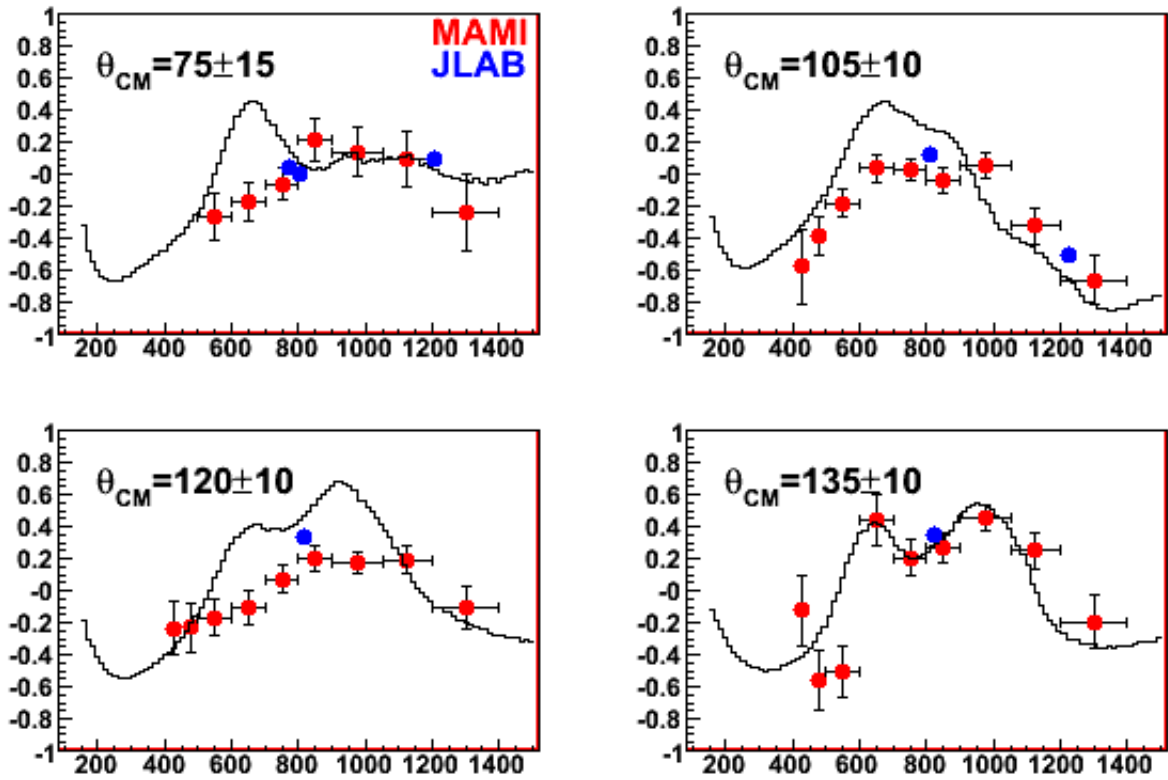
Figure 10: Preliminary results for $C_{x'}$ in the p($\gamma, p\pi^0$) reaction from the Phase-I polarimeter. The x-axis is the incident photon energy (MeV) and the y-axis is the observable $C_{x'}$. The published data from JLAB are also shown on the plot. The solid line is the prediction of the SAID PWA.
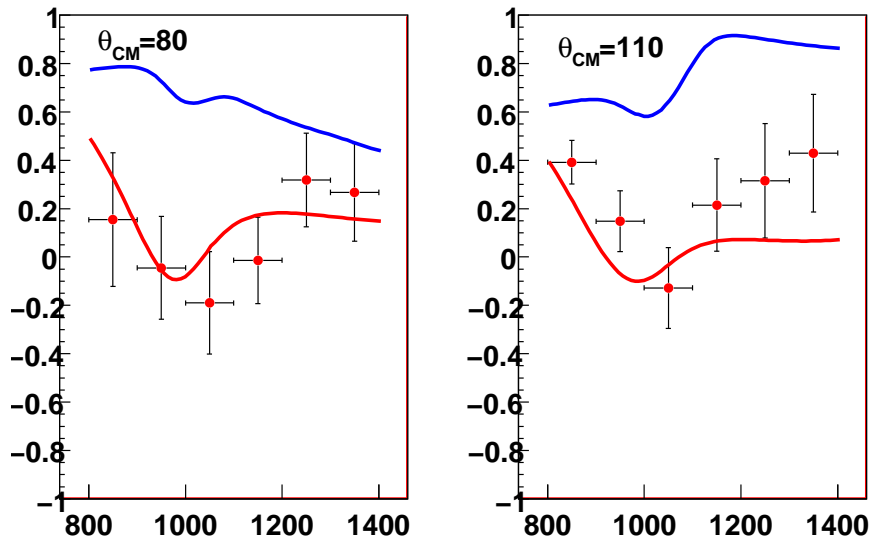
Figure 11: Preliminary results for $C_{x'}$ in the p($\gamma, p\eta$) reaction from the Phase-I polarimeter. The x-axis is the incident photon energy (MeV) and the y-axis is the observable $C_{x'}$. The red (blue) solid line is the prediction of the SAID (MAID)PWA.
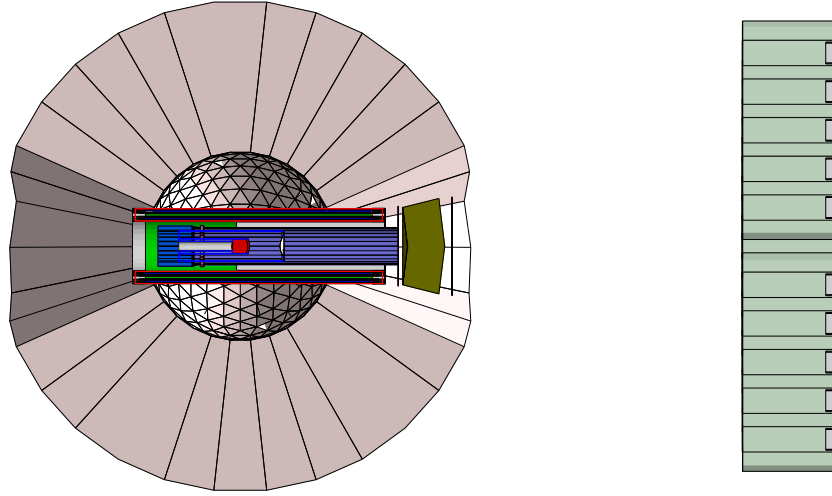
Figure 12: GEANT4 picture of phase-II polarimeter setup. As well as the Crystal Ball and TAPS detectors also shown are the target (red), PID (blue), graphite analysing material (grey) and MWPC (red/ bright green). The forward plug is shown in dark green.

2.4 Phase-II Nucleon polarimeter design

2.4.1 Central angle region

The phase-I design has proven very successful. However it has a drawback in that the use of kinematic tracking limits its applicability to free proton targets where the reacting nucleon is initially stationary. Extending the measurements to neutron targets requires a modified design, because of the unavoidable Fermi motion of the target neutrons. Also the phase-I design does not provide polarimetry information on neutrons.

The new Phase-II polarimeter addresses both these issues. It exploits the PID, the Pavia wire chambers and a new active forward angle scatterer. The design is outlined below and illustrated in Fig 12. The analysing material, comprising a cylinder of 1.5cm thick graphite, will be sandwiched between the PID plastic scintillator barrel and the wire chambers. Full track information will then be available for protons exiting the graphite. The PID will enable discrimination between proton and neutron as well as some information on the phi angle of the incident proton tracks. The wire chamber is moved downstream by $\sim$5 cm to increase the coverage down to $\sim$15°.

For protons incident on the polarimeter the proposed device can characterise the emerging track from ^{12}C(p,p$^{/}$) scatter events with a resolution of $\sim$2°. Knowlege of this track is sufficient to select the nuclear scattered events of interest even in the case where Fermi motion plays a role at the reaction vertex, as indicated in the results of the Geant simulation (Sec 3).

The design will also utilise ^{12}C(n,p) charge exchange reactions, where the proton from the charge exchange scatter will give the polarimetry information for the incident neutrons.
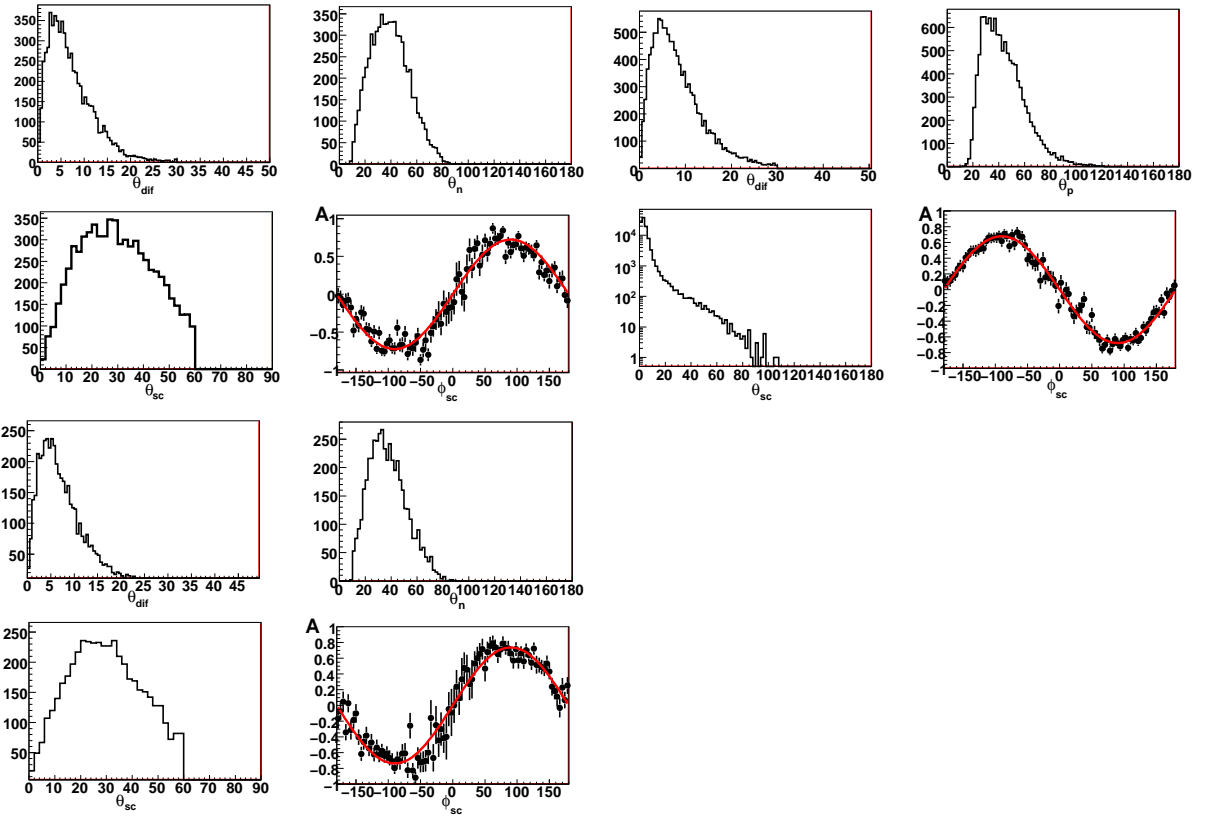
Figure 13: 4 panels top left: θ_{diff}, $\theta_{nucleon}$, θ_{scat} and dilution of analyzing power for simulation of phase-II polarimeter for the p$(\gamma, \pi^+)n$ reaction. 4 panels top right same plots for D(p)$(\gamma, \pi^0)p$. 4 panels bottom right: same plots for D(p)$(\gamma, \pi^+)n$

2.4.2 The forward region

The central polarimeter gives polarimetry information down to nucleon lab angles of $\sim 15°$. The acceptance in the forward region will be covered by an additional polarimeter. The design of the polarimeter for this small forward angle acceptance region is currently being finalised, but would likely comprise a segmented active plastic scintillator scatterer with the segmented TAPS detector acting as the detector for the scattered nucleons. Light deposited in the segments of the scatterer will be passed by optical fibres to a multianode photomultiplier tube to provide hit and energy information, registering $CH_2(n,p)$ and $CH_2(n,n)$ scatters. This light readout system will use optical fibres and be similar to that employed for the TAPS veto detectors [19]. The expected position of the forward polarimeter is shown in Fig. 12.

3 GEANT4 simulations of the proposed setup

The proposed setup has been simulated using a realistic physics event generator based on the SAID partial wave analysis. These events are passed through a realistic Geant4 model of the A2 detector apparatus.

The proposed setup has been simulated with a realistic physics event generator based on the SAID partial wave analysis. The simulation can generate quasi free pion production from a stationary nucleon or incorporate Fermi motion of a nucleon in deuterium with realistic momentum distribution inferred from $D(e, e'p)$. The results of the analysis are shown in Figure 13 for the $p(\gamma, \pi^+)n$, $D(p)(\gamma, \pi^0)p$ and $D(p)(\gamma, \pi^+)n$ reactions. These channels were chosen to test the capabillity of the polarimeter to work for deuterium targets (Fermi motion) and to model the expected capability for neutron polarimetry. The incident nucleon track from the target was reconstructed from the vector joining the centre of the target and the hit position in the wire chambers while the scattered nucleon track following the graphite is given by the wire chambers. For each channel 4 spectra are presented these are: (i) θ_{diff} - the angle between the incident nucleon and that reconstrcted from the γ and meson 4-vectors (ii) θ_n the lab angle of the nucleon (iii) θ_{sc} the reconstructed scatter angle of the nucleon in the graphite and (iv) A - the reconstructed azimuthal asymmetry of the scattered nucleons. For the simulation the analysing power and C_x were both set to unity so any deviation from unity in the reconstructed azimuthal asymmetry reflects dilution of the analyzing power.

The simulation results confirm the expected capability of the polarimeter. The dilution of the analyzing power because of the experimental resolution and any contamination in the selection of nuclear scatter events is small and well established amounting to at most $\sim 25\%$. This dilution is expected to be reduced further with a more refined analysis of the data for the actual experiment. The efficiency of the polarimeter for proton scattering events is $\sim 3\%$ and for (n,p) charge exchange events is $\sim 1\%$. These figures are used in the count rate estimate.

4 Event rates and beamtime estimate

The measurement of $C_{x'}$, $O_{x'}$, T and P will be obtained in the same experiment using a photon beam which has both circular and linear polarisation

We request a beam time of 960 hours to obtain adequate statistics for double-polarisation observables in both π and η photoproduction in an E_γ bin of ± 25 MeV and a θ_{meson} bin of $\pm 10°$. The expected statistical errors calculated according to this beamtime are outlined below.

The estimate was made using the following input:

- **Tagged photon flux:** A tagged photon rate of 1.25×10^5 $\gamma \mathrm{s}^{-1}\mathrm{MeV}^{-1}$.

- **Target:** The liquid hydrogen target is assumed to contain 2.1×10^{23} nuclei/cm^2

- **Cross sections:** We typically expect cross sections as low as 3μb/sr for π photoproduction and 0.7μb/sr for η production.

- **Meson detection efficiencies:** A value of ϵ_{meson}=80% was taken for π° and ϵ_{meson}=35% for η detection

- **Data acquisition system live time:** $\epsilon_{DA} \sim$**70%**

- **Proton Polarimetry characteristics:** Protons: The probability for a "useful" nucleon scatter in the graphite with angles between 10-30° ($\epsilon^p_{polarimeter}$ is taken to be 3%. The average analysing power for the polarimeter is taken to be 0.2 for proton scattering.

- **Neutron Polarimeter efficiency:** The probability for a "useful" (n,p) scatter in the graphite with angles between 10-30° ($\epsilon^n_{polarimeter}$ is indicated by the G4 simulation to be $\sim$1%. The average analysing power for the polarimeter is ~ 0.1 for neutron scattering.

- **Scattered nucleon count rate:** Therefore the number of usefully scattered nucleons incident on the polarimeter with a θ_{meson} bin of $\pm 10^\circ$ having typical solid angle Ω_{avg} of 1 sr. and a photon energy bin of width ± 25 MeV in a beamtime of t seconds is given by :

$$N_{nucleons} = \sigma^N_{polarimeter} \times 2.5 \times 10^5 \times 50 \times 2.1 \times 10^{23} \times \sigma_{avg} \times \Omega_{avg} \times \epsilon_{meson} \times \epsilon_{DA} \times t$$

- **Accuracy of C$_{x'}$** The absolute statistical error in the polarisation observables can be determined from the formula $\Delta C_{x'} \sim \sqrt{(\frac{2}{A^2 N})}$ where A is the product of the analysing power of the polarimeter and the degree of circular polarisation of the beam and N is the number of usefully scattered nucleons incident on the polarimeter. Results are shown in the table below.

- **Accuracy of O$_{x'}$:** Absolute statistical error obtained from the formula $\Delta O_{x'} \sim \frac{2}{\sqrt{(A^2 N)}}$ where A is the product of the analysing power of the polarimeter and the degree of linear polarisation of the beam. This error also applies to the extraction of the single polarisation observable T. Results are shown in the table.

- **Accuracy of P**: Absolute statistical error obtained from the formula $\Delta P \sim \frac{2}{\sqrt{(A^2 N)}}$ where A is the analysing power of the polarimeter alone.

	σ_{avg}	$N_{scattered}$	$\vec{P}^{linear}$	$\vec{P}^{circ}$	$\Delta O_{x'}$	$\Delta C_{x'}$	ΔP
$E_e=$ 1500 MeV $p(\gamma,p)\pi^0$	$3(\mu\mathrm{b/sr})$	21.9×10^4	E_γ=0.4-0.6: 0.4	E_γ=0.4-1.5: 0.5	0.04	0.02	0.01
$E_e=$ 1500 MeV $n(\gamma,n)\pi^0$	$3(\mu\mathrm{b/sr})$	7.32×10^4	E_γ=0.4-0.6: 0.4	E_γ=0.4-1.5: 0.5	0.15	0.09	0.04
E_e=1500 MeV $n(\gamma,n)\eta$	$0.7(\mu\mathrm{b/sr})$	3.2×10^4		E_γ=0.8-1.5: 0.7		0.1	0.07
$E_e=$ 1500 MeV $D(\gamma,p)n$	$0.3(\mu\mathrm{b/sr})$	1.7×10^4	E_γ=0.4-0.6: 0.4	E_γ=0.4-1.5: 0.5	0.19	0.08	0.04

Total Production beam time - 960 hrs with E_e=1500 MeV

We would also require beamtime to commission the nucleon polarimeter before the main production run. From the estimates above, a test beamtime of 100 hours would give sufficient statistics to establish the polarimeter capabilities and optimise the design.

Nucleon polarimeter commissioning beam time - 100 hrs

References

[1] E Klempt, H-H Richard, arXiv:0901.2055v1 (2009)

[2] F.X. lee *et. al.*, hep-lat/0208070

[3] T.D. Cohen and L.Y. Glozman, Int. Journ. Mod. Phys. A17, 1327 (2002)

[4] Guy F. de Teramond and Stanley J. Brodsky, Phys. Rev. Lett. 94, 201601 (2005)

[5] J. Ahrens *it. al.*, Phys. Rev. Lett. 88, 232002 (2002)

[6] D. Dutta, H. Gao and T-S H Lee, Phys. Rev. C 65 (2002) 044619;

[7] W. Roberts et. al., W. Roberts and T. Oed, Phys. Rev. C 71, 055201 (2005).

[8] K. Wijesooriya *et. al.*, Phys. Rev. C 66 (2002) 034614;

[9] A. Bock *et. al.*, Phys. Rev. Lett. 81, 534?537 (1998)

[10] J.Ajaka *et. al.*, Phys. Rev. Lett. 81, 1797?1800 (1998)

[11] Avakyan et. al., Soviet Journal Nucl. Phys. 53, 448(1991)

[12] http://gwdac.phys.gwu.edu/

[13] R. Novotny, IEEE Trans. Nucl. Sci. A **38**, 379 (1991).

[14] Th. Pospischil *et. al.*, Nucl. Inst. and Meth. A 483 (2002) 713.

[15] A. Fix, Private communication (2008)

[16] K. Livingston (Univ of Glasgow), Private communication.

[17] J. Ball et. al., Nucl Phys. A559 (1993)

[18] M. Schwamb and H. Arenhovel, Nucl. Phys. A690 p682 (2001)

[19] S. Jannsen et. al., IEEE TRANSACTIONS ON NUCLEAR SCIENCE, VOL. 47, NO. 3, JUNE 2000

[20] K. Wisejoorya et. al., Phys. Rev. Lett 86, 2975 (2001)

[21] Th. Pospischil et al., Nucl. Instr. and Meth. A 483 (2002) 713-725

[22] J. Alcorn et. al. Nucl. Instr. and Meth. in Phys. Res. A 522 (2004) 294346

[23] F. Adamian et. al., J. Phys. G: Nud. Phys. 14 (1988) 831-833.

[24] Eur. Phys. Journ. A39, 149 (2009)

[25] T. Wakasa, Nucl.Instrum.Meth. A547 (2005) 569-582

5 Experimental apparatus

5.1 Photon Beam

The A2 photon beam is derived from the production of Bremsstrahlung photons during the passage of the MAMI electron beam through a thin radiator. The resulting photons can be circularly polarised, with the application of a polarised electron beam, or linearly polarised, in the case of a crystalline radiator. The degree of polarisation achieved is dependent on the energy of the incident photon beam (E_0) and the energy range of interest, but currently peaks at ∼75% for linear polarisation (Fig. 14) and ∼85% for circular polarisation (Fig. 15). The maximum degree of linear polarisation should be further improved by 5 to 10% by the end of 2009 when the collimation and beam monitoring systems will be optimised for MAMI-C during the installation of the Frozen Spin Target. The Glasgow Photon Tagger (Fig 16) provides energy tagging of the photons by detecting the post-radiating electrons and can determine the photon energy with a resolution of 2 to 4 MeV depending on the incident beam energy, with a single-counter time resolution $\sigma_t = 0.117$ ns [2]. Each counter can operate reliably to a rate of ∼1 MHz, giving a photon flux of $2.5 \cdot 10^5$ photons per MeV. Photons can be tagged in the momentum range from 4.7 to 93.0% of E_0.
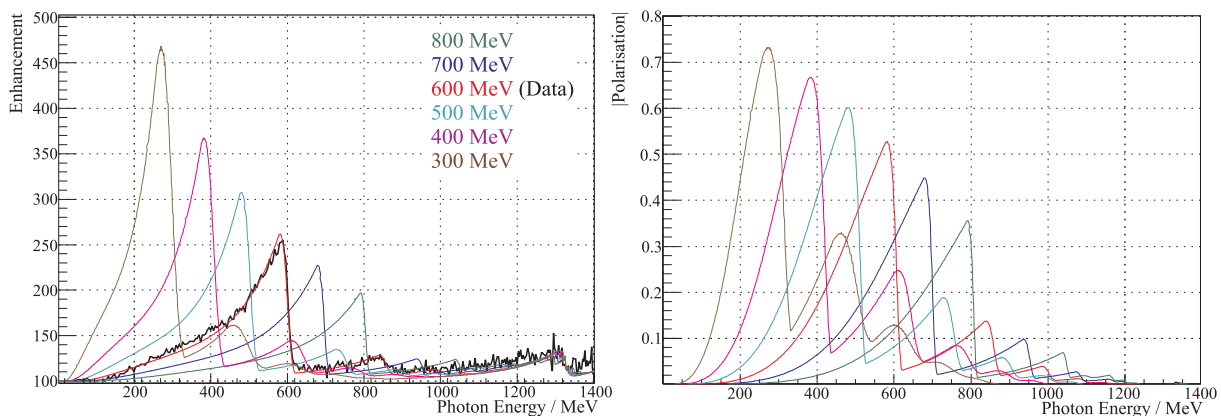

Figure 14: Linear polarisation available with the current collimation system for a variety of crystal orientations. The thin black lines are data obtained during recent MAMI-C runs.

To augment the standard focal plane detector system and make use of the Tagger's intrinsic energy resolution of 0.4 MeV (FWHM), there exists a scintillating fibre detector ('Tagger Microscope') that can improve the energy resolution by a factor of about 6 for a ∼100 MeV wide region of the focal plane (dependent on its position) [4].

5.2 Frozen-Spin Target

Polarisation experiments using high density solid-state targets in combination with tagged photon beams can reach the highest luminosities. For the double polarisation measurements planned with the Crystal Ball detector on polarised protons and deuterons a specially designed, large horizontal ^{3}He/^{4}He dilution refrigerator was built in cooperation with the Joint Institute for Nuclear Research (JINR) Dubna (see Figure 17). It has minimum limitations for the particle detection and fits into the central core of the inner Particle Identification Detector (PID2). This was achieved by using the frozen spin technique with the new concept of placing a thin superconducting holding coil inside the polarisation refrigerator. Longitudinal and transverse polarisations will be possible.

Highest nucleon polarisation in solid-state target materials is obtained by a microwave pumping
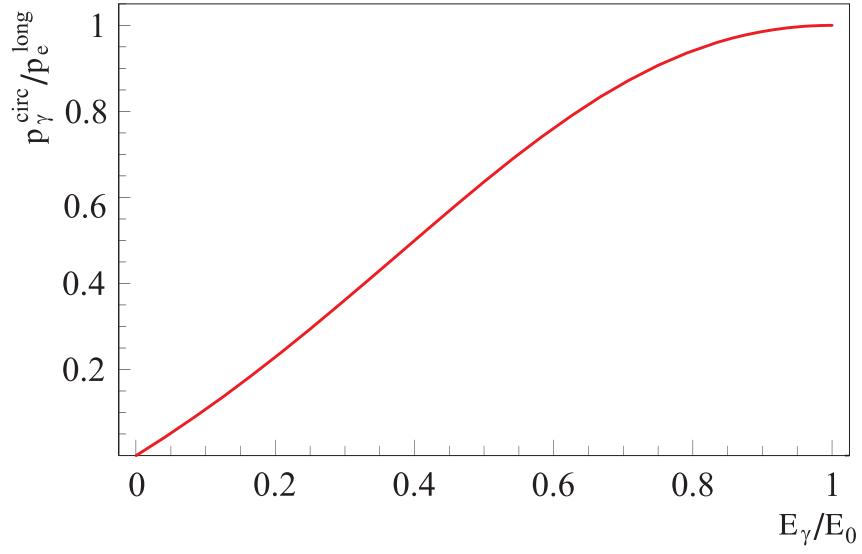
Figure 15: Helicity transfer from the electron to the photon beam as function of the energy transfer. The MAMI beam polarisation is $P_e \approx 85\%$.
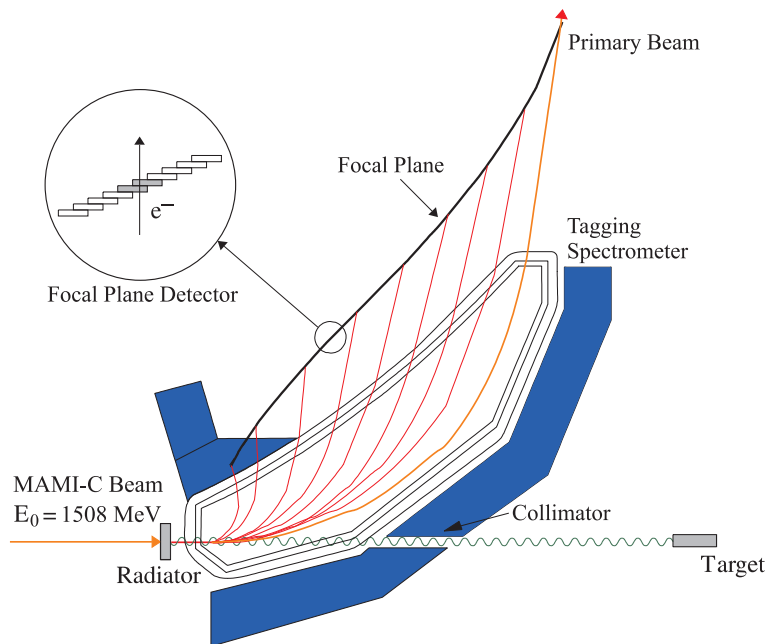

Figure 16: The Glasgow photon tagging spectrometer.

Figure 17: The new dilution refrigerator for the Crystal Ball Frozen Spin Target.

process, known as 'Dynamic Nucleon Polarisation' (DNP). This process is applicable to any nucleus with spin and has already been used in different experiments with polarised proton and deuteron targets. The geometric configuration of the target is the same for the polarised proton and neutron setup. However, since the polarisation measurement of the deuteron is more delicate due to the small size of the polarisation signals, the modification of some basic components is needed. The reason for this is twofold: firstly the magnetic moment of the deuteron is smaller than that of the proton and, in addition, the interaction of the deuteron quadrupole moment with the electric field gradient in the sample broadens the deuteron polarisation signal. An accuracy $\delta P_p/P_p$ of 2 to 3% for the protons and $\delta P_D/P_D$ of 4 to 5% for the deuterons is expected in the polarisation measurement. It has also to be taken into account that the measured deuteron polarisation P_D is not equal to the neutron polarisation P_n. Assuming a 6 % admixture of the D-state of the deuteron, a calculation based on the Clebsch-Gordon coefficients leads to $P_n = 0.91 \, P_D$. Several polarised proton and deuteron materials are available such as alcohols and deuterated alcohols (e.g. butanol C_4H_9OH), NH_3, ND_3 or ^6LiD. The most important criteria in the choice of material suitable for particle physics experiments are the degree of polarisation P and the ratio k of free polarisable nucleons to the total number of nucleons. Further requirements on polarised target materials are a short polarisation build-up time and a simple, reproducible target preparation. The polarisation resistance against radiation damage is not an issue for experiments with a low intensity tagged photon beam ($\dot{N}_\gamma \approx 5 \cdot 10^7$ s^{-1}) as will be used here. However, the limitations of a reduced relaxation time due to overheating of the target beads (Kapitza resistance) will have to be investigated.

Taking all properties together, butanol and deuterated butanol are the best material for this experiment. For protons we expect a maximum polarisation of $P_p = 90\%$ and an average polarisation of $P_p = 70\%$ in the frozen spin mode. Recently, a deuteron polarisation $P_D = 80\%$

was obtained with Trityl doped butanol targets at 2.5 T magnetic field in a ^{3}He/^{4}He dilution refrigerator. At a 0.4 T holding field an average neutron polarisation P_n (see above) of 50 % will be obtained. The filling factor for the $\sim$2 mm diameter butanol spheres into the 2 cm long, 2 cm diameter target container will be around 60%. The experience from the GDH runs in 1998 [5] shows that, with a total tagged photon flux of $5 \cdot 10^7$, relaxation times of about 200 hours can be expected. The polarisation has to be refreshed by microwave pumping every two days. In conclusion, we estimate that we will achieve the following target parameters:

- Maximum total tagged photon flux in the energy range of 4.7 to 93% of E_0: $\dot{N}_\gamma \approx 5 \cdot 10^7 \, \text{s}^{-1}$, with relaxation time of 200 hours.

- Target proton density in 2 cm cell: $N_T \approx 9.1 \cdot 10^{22} \text{cm}^{-2}$ (including dilution and filling factors)

- Average proton polarisation $P_p = 70\%$

- Target deuteron density in 2cm cell: $N_T \approx 9.4 \cdot 10^{22} \text{cm}^{-2}$ (including dilution and filling factors)

- Average neutron polarisation $P_n = 50\%$

5.3 Crystal Ball Detector System

The central detector system consists of the Crystal Ball calorimeter combined with a barrel of scintillation counters for particle identification and two coaxial multiwire proportional counters for charged particle tracking. This central system provides position, energy and timing information for both charged and neutral particles in the region between $21°$ and $159°$ in the polar angle (θ) and over almost the full azimuthal (ϕ) range. At forward angles, less than $21°$, reaction products are detected in the TAPS forward wall. The full, almost hermetic, detector system is shown schematically in Fig. 18 and the measured two-photon invariant mass spectrum is shown in Fig. 19.

The Crystal Ball detector (CB) is a highly segmented 672-element NaI(Tl), self triggering photon spectrometer constructed at SLAC in the 1970's. Each element is a truncated triangular pyramid, 41 cm (15.7 radiation lengths) long. The Crystal Ball has an energy resolution of $\Delta E/E = 0.020 \cdot E[GeV]^{0.36}$, angular resolutions of $\sigma_\theta = 2 \ldots 3°$ and $\sigma_\phi = \sigma_\theta / \sin \theta$ for electromagnetic showers [1]. The readout electronics for the Crystal Ball were completely renewed in 2003, and it now is fully equipped with SADCs which allow for the full sampling of pulse-shape element by element. In normal operation, the onboard summing capacity of these ADCs is used to enable dynamic pedestal subtraction and the provision of pedestal, signal and tail values for each element event-by-event. Each CB element is also newly equipped with multi-hit CATCH TDCs. The readout of the CB is effected in such a way as to allow for flexible triggering algorithms. There is an analogue sum of all ADCs, allowing for a total energy trigger, and also an OR of groups of sixteen crystals to allow for a hit-multiplicity second-level trigger - ideal for use when searching for high multiplicity final states.

In order to distinguish between neutral and charged particles species detected by the Crystal Ball, the system is equipped with PID2, a barrel detector of twenty-four 50 mm long, 4 mm thick scintillators, arranged so that each PID2 scintillator subtends an angle of $15°$ in ϕ. By matching a hit in the PID2 with a corresponding hit in the CB, it is possible to use the locus of the $\Delta E, E$ combination to identify the particle species (Fig. 20). This is primarily used for the separation of charged pions, electrons and protons. The PID2 covers from $15°$ to $159°$ in θ.

The excellent CB position resolution for photons stems from the fact that a given photon triggers several crystals and the energy-weighted mean of their positions locates the photon position to better than the crystal pitch. For charged particles which deposit their energy over only one or
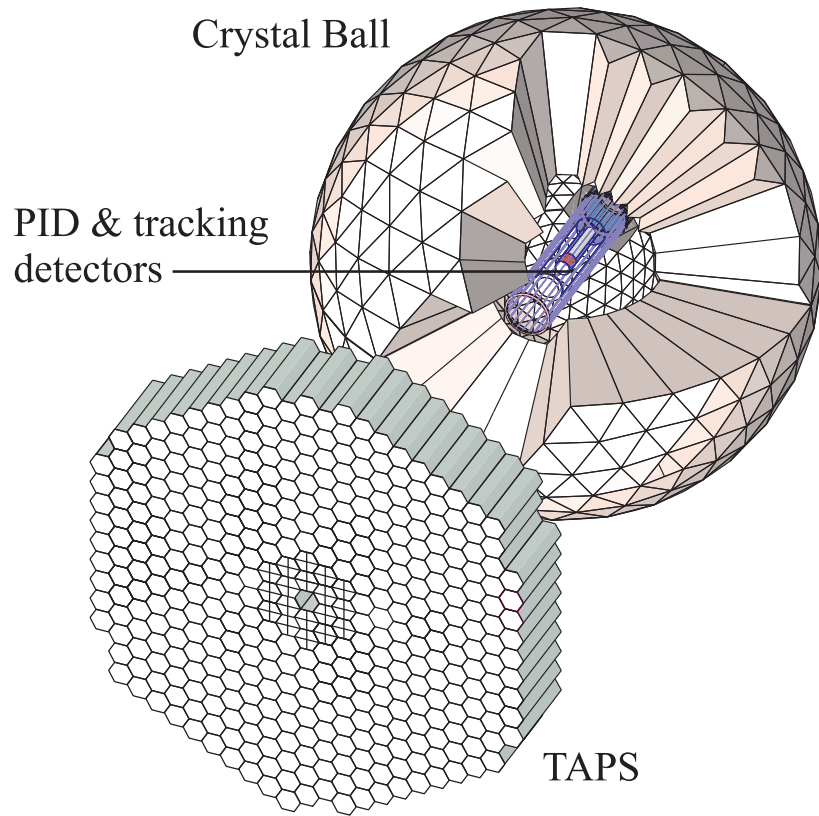
Figure 18: The A2 detector setup: The Crystal Ball calorimeter, with cut-away section showing the inner detectors, and the TAPS forward wall.
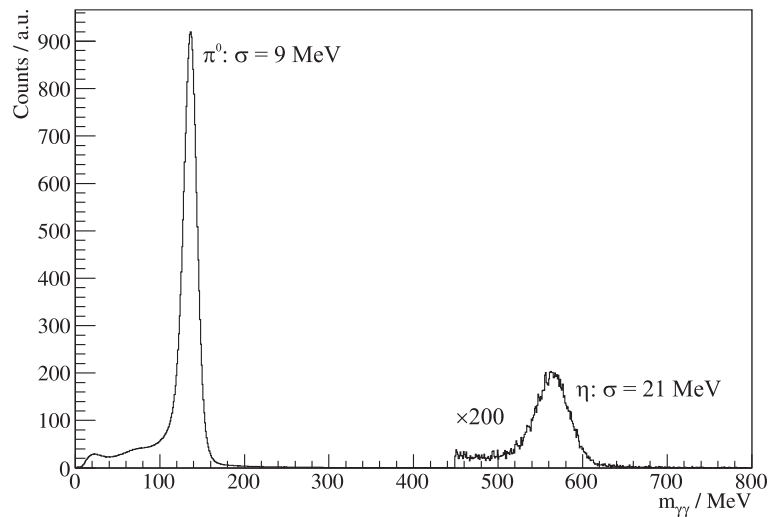

Figure 19: Two photon invariant mass spectrum for the CB/TAPS detector setup. Both η and π^0 mesons can be clearly seen.
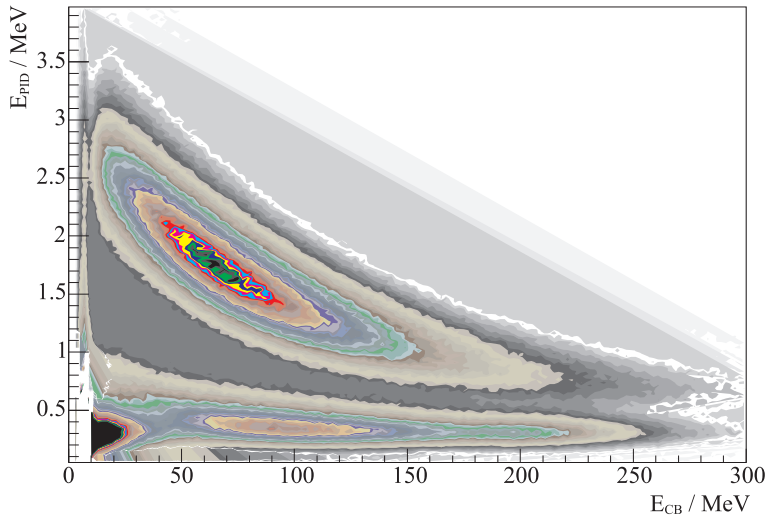
Figure 20: A typical $\Delta E/E$ plot from the Crystal Ball and the PID2 detector. The upper curved region is the proton locus, the lower region contains the pions and the peak towards the origin contains mostly electrons.

two crystals, this is not so precise. Here the tracks of charged particles emitted within the angular and momentum acceptance of the CB detector will be reconstructed from the coordinates of point of intersections of the tracks with two coaxial cylindrical multiwire proportional chambers (MWPCs) with cathode strip readout. These MWPCs are similar to those installed inside the CB during the first round of MAMI-B runs [3]. The most significant difference is that all detector signals are taken at the upstream end of the MWPCs, minimising the material required and facilitating particle detection in the forward polar region.

A mixture of argon (79.5%), ethane (30%) and freon-CF_4 (0.5%) is used as the filling gas. This mixture is a compromise between charge multiplication and localization requirements imposed by the ionizing particle tracks.

Within each chamber both the azimuthal and the longitudinal coordinates of the avalanche will be evaluated from the centroid of the charge distribution induced on the cathode strips. The location of the hit wires(s) will be used to resolve ambiguities which arise from the fact that each pair of inner and outer strip cross each other twice. The expected angular resolution (rms) will be $\sim 2°$ in the polar emission angle θ and $\sim 3°$ in the azimuthal emission angle ϕ.

The MWPCs have been recently installed inside the CB frame and their calibration using both cosmic rays and test beam data is currently underway.

5.4 TAPS Forward Wall

The TAPS forward wall is composed of 384 BaF_2 elements, each 25 cm in length (12 radiation lengths) and hexagonal in cross section, with a diameter of 59 mm. The front of every TAPS element is covered by a 5 mm thick plastic veto scintillator. The single counter time resolution is $\sigma_t = 0.2$ns, the energy resolution can be described by $\Delta E/E = 0.018 + 0.008/E[GeV]^{0.5}$ [1]. The angular resolution in the polar angle is better than $1°$, and in the azimuthal angle it improves with increasing θ, being always better than $1/R$ radian, where R is the distance in centimeters from the central point of the TAPS wall surface to the point on the surface where the particle trajectory meets the detector. The TAPS readout was custom built for the beginning of the CB@MAMI program and is effected in such a way as to allow particle identification by Pulse Shape Analysis (PSA), Time Of Flight (TOF) and $\Delta E/E$ methods (using the energy deposit in the plastic scintillator to give ΔE). TAPS can also contribute to the CB multiplicity trigger

and is currrently divided into upto six sectors for this purpose. The 2 inner rings of 18 BaF$_2$ elements have been replaced recently by 72 PbWO$_4$ crystals each 20 cm in length (22 radiation lengths). The higher granularity improves the rate capability as well as the angular resolution. The crystals are operated at room temperature. The energy resolution for photons is similar to BaF$_2$ under these conditions [6].

References

[1] S. Prakhov et al.: *Measurement of the Slope Parameter α for the $\eta \rightarrow 3\pi^0$ decay with the Crystal Ball dectector at the Mainz Microtron (MAMI-C)*, Phys. Rev. **C 79** (2009) 035204

[2] J.C. McGeorge et al.: *Upgrade of the Glasgow photon tagging spectrometer for Mainz MAMI-C*, Eur. Phys. J. **A 37** (2008) 129

[3] G. Audit et al.: *DAPHNE: a large-acceptance tracking detector for the study of photoreactions at intermediate energies*, Nucl. Instr. Meth. **A 301** (1991) 473

[4] A. Reiter et al.: *A microscope for the Glasgow photon tagging spectrometer in Mainz*, Eur. Phys. J. **A 30** (2006) 461

[5] A. Thomas et al.: *The GDH Experiment at MAMI*, Nucl. Phys. **B 79** (1999) 591

[6] R. Novotny *et al.*: *Scintillators for photon detection at medium energies: A comparative study of BaF-2, CeF-3 and PbWO-4*, Nucl. Instrum. Meth. A **486** (2002) 131